ELSEVIER

Electrochemical and thermal behavior of aluminum- and magnesium-doped spherical lithium nickel cobalt mixed oxides $Li_{1-x}(Ni_{1-y-z}Co_yM_z)O_2$ (M = Al, Mg)

S. Albrecht[a,*], J. Kümpers[b], M. Kruft[a], S. Malcus[a], C. Vogler[c], M. Wahl[b], M. Wohlfahrt-Mehrens[c]

[a]*H.C. Starck GmbH, Im Schleeke 78-91, D-38642 Goslar, Germany*
[b]*NBT GmbH, Am Leineufer 51, D-30419 Hannover, Germany*
[c]*ZSW—Center for Solar Energy and Hydrogen Research, Baden-Württemberg—Div. 3, Helmholtzstraße 8, D-89081 Ulm, Germany*

Abstract

An industrial synthesis process for spherical lithium nickel cobalt mixed oxides, $Li(Ni_{1-y}Co_y)O_2$, has been successfully applied to aluminum- and magnesium-doped lithium nickel cobalt mixed oxides $Li(Ni_{1-y-z}Co_yM_z)O_2$ (M = Al, Mg). The additional elements stabilize the layered structure and enhance the cycling stability. The decomposition temperature of charged electrodes depends on the delithiation state and the crystallite size but not directly on the content of dopants. Therefore, enhancement of the thermal stability by aluminum and magnesium seems mainly to be an indirect effect due to an intrinsic limitation of the delithiation.
© 2003 Elsevier Science B.V. All rights reserved.

Keywords: Lithium nickel cobalt mixed oxides; Cycling stability; Charged electrodes

1. Introduction

The solid solution series of lithium nickel cobalt mixed oxides, $Li(Ni_{1-y}Co_y)O_2$, comprises very promising positive electrode materials for high energy and high power lithium-ion batteries [1,2]. They provide a compromise between the good cyclability, reproducibility, and thermal stability of lithium cobalt oxide $LiCoO_2$, and the high capacity and the lower prize of lithium nickel oxide $LiNiO_2$. According to the open literature the most advantageous compositions range from $y = 0.2$ to 0.3 [3,4]. However, there are still some safety and cyclability concerns existent. Safety problems arise from the instability of the delithiated "NiO_2" phase releasing oxygen at elevated temperatures. In the case of lithium nickel oxides, $Li_{1-x}(Ni_{1-y}M_y)O_2$, it is known that thermal stability in the charged state and cyclability can be enhanced by aluminum [5–8] or magnesium doping [9,10].

Positive electrode materials of spherical particle morphology contain technological advantages with respect to the synthesis of the material as well as during electrode preparation, and are therefore preferred [11]. H.C. Starck has developed an industrial synthesis process for the manufacture of spherical lithium nickel cobalt mixed oxides $Li(Ni_{1-y}Co_y)O_2$ (first generation) [12]. Aim of the presented work was to apply this process to aluminum- and magnesium-doped lithium nickel cobalt mixed oxides $Li(Ni_{1-y-z}Co_yM_z)O_2$ (M = Al, Mg) (second generation), and to analyze and optimize these materials for the intended battery application.

2. Experimental procedures

2.1. Synthesis procedure

Stoichiometric amounts of a Li-compound, a spherical, Co-doped Ni-compound and a compound of the dopant (Mg or Al) are mixed in an initial stage. The resulting precursor is successively calcined for numerous hours at constant temperature (>600 °C) applying a continuous flow of purging gas (N_2, O_2, air). Conversion of the precursor into the mixed oxide by calcination is followed by a final conditioning (particle size adjustment) of the mixed lithium transition oxide.

2.2. Composition ranges for synthesis

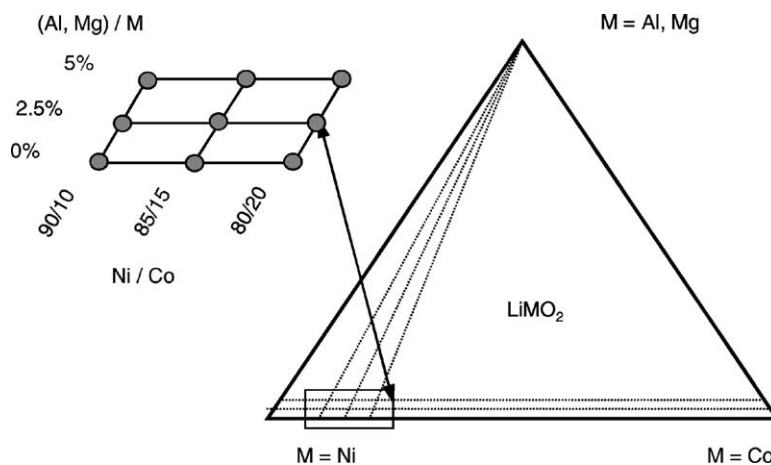Fig. 1 illustrates the composition matrix as points within the composition diagram $LiMO_2$ (M = Ni, Co, Al/Mg). The

---

Fig. 1. Nominal compositions of the samples of this study within the ternary systems $LiMO_2$ (M = Ni, Co, Al/Mg).

maximum cobalt content was set to 20 mol% due to economic reasons. The minimum cobalt content adjusted was 10 mol% and the maximum aluminum and magnesium contents were set to 5 mol%, according to the literature mentioned above. Within these composition limits, sample compositions were set to intersection points of lines of constant Ni/Co ratio and lines of constant aluminum and magnesium content, respectively.

2.3. Structural characterization

X-ray diffraction profiles of the samples were measured with a Siemens D5000 diffractometer (Cu Kα radiation, graphite secondary monochromator).

Structural parameters were determined by Rietveld analysis of diffraction profiles, using the Bruker AXS program Win-Rietveld. Since lithium is a weak X-ray scatterer, and since there are strong correlations among some of the structural parameters, certain approximations are necessary. It is supposed that aluminum and cobalt exclusively occupy cation positions in the nickel layers, and that there is no site vacancy. Magnesium was supposed to be able to occupy not only nickel positions, but also lithium positions, according to the structure and chemical similarities of lithium and magnesium. For the lithium nickel disorder a simple partial replacement of lithium ions within the lithium layers by nickel ions was presumed.

2.4. Cycling test

Selected materials were electrochemically characterized at NBT using 2025 coin cells. Half-cells comprising a Li metal anode have been assembled and tested in order to determine the specific capacity of cathode materials. Based on the half-cell results, full coin cells have been assembled. Full coin cells consist of a MCMB-6-28 anode on a nickel foam substrate and a cathode pellet with 80 wt.% active material, 10 wt.% PTFE and 10 wt.% conductive agent. Cells were cycled at constant temperature of 23 °C with a

C/15 current rate for charge and discharge, respectively. Cells were cycled until the capacity reached 80% of its initial value. With regard to the cycling stability of prismatic or round type Li-ion cells full coin cells give more realistic results than half-cells.

2.5. Thermal measurements

For thermal measurements, positive electrodes were charged versus lithium metal in three-electrode Teflon cells at a constant temperature of 23 °C. Merck's LP30 was used as electrolyte. After performing three galvanostatic half-cycles between 3.0 and 4.3 V versus Li/Li^+ at a constant current of C/20, the cells were potentiostatically charged at 4.3 V versus Li/Li^+ for 12 h. Cells were disassembled in an argon box, the positive electrodes washed in DMC, dried overnight in the argon box, and successively sealed in aluminum cans for simultaneous thermal analysis (STA). By this method, differential scanning calorimetry (DSC) and thermal gravimetry (TG) are applied simultaneously, allowing a simultaneous measurement of changes in the sample's enthalpy and weight. Experiments were performed up to a temperature of 400 °C with a heating rate of 10 K/min applying argon as purging gas.

3. Results and discussion

3.1. Morphology

All samples of this study have spherical particle morphology (Fig. 2). The spheroids themselves are composed of regular, corner and edge truncated crystallites and have a certain internal porosity, which improves electrolyte access. The size of the crystallites strongly depends on the synthesis temperature, whereas the size of the spheroids is unaffected by the synthesis temperature. Fig. 3 gives an example of the crystallite size enlargement, which is obtained when the synthesis temperature is increased by 50 K.
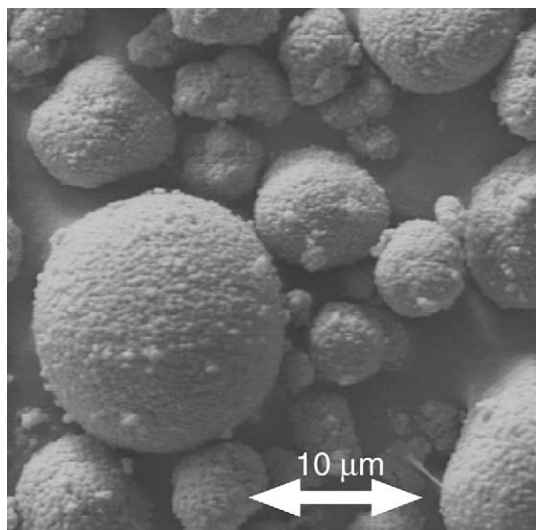
Fig. 2. SEM picture of spherical aluminum-doped lithium nickel cobalt mixed oxide LiNi$_{0.865}$Co$_{0.110}$Al$_{0.025}$O$_2$.
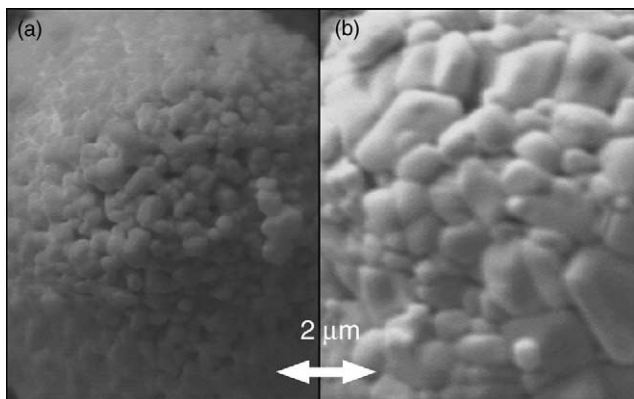

Fig. 3. SEM picture of spherical aluminum-doped lithium nickel cobalt mixed oxide LiNi$_{0.80}$Co$_{0.15}$Al$_{0.05}$O$_2$. (a) Standard synthesis; (b) synthesis temperature increased by 50 K.
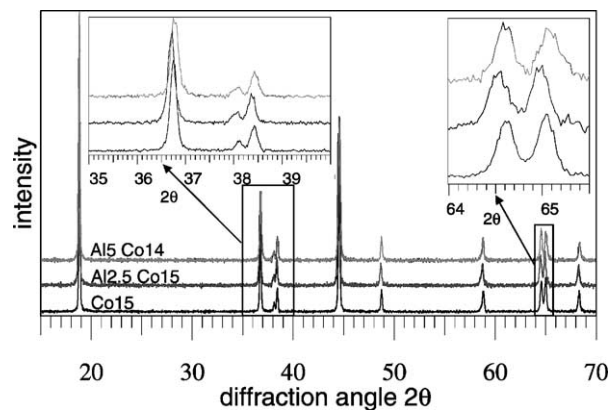

Fig. 4. X-ray diffraction spectra of aluminum-doped mixed oxides (selection).
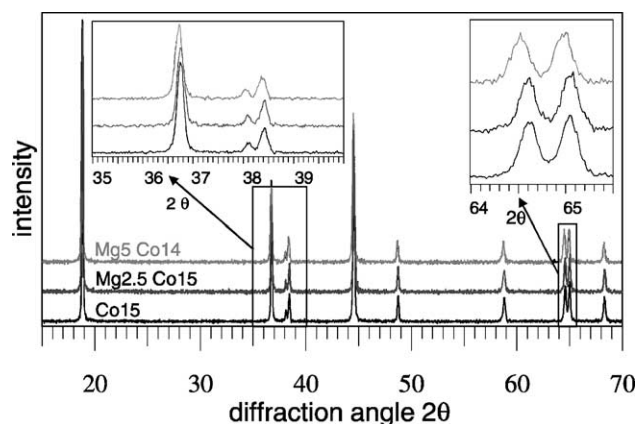
Fig. 5. X-ray diffraction spectra of magnesium-doped mixed oxides (selection).

3.2. Structural properties

Figs. 4 and 5 show examples of X-ray diffraction spectra of aluminum- and magnesium-doped mixed oxides. In the X-ray diffraction spectra of all samples, all diffraction lines can be indexed to space group $R\bar{3}m$ and are attributed to a single-layered structure phase. No other diffraction lines are visible in the spectra. Additionally, the profiles of the diffraction lines are quite narrow and no shoulders appear, indicating a homogeneous distribution of each element. Chemically and structurally homogeneous, single-phase materials have been obtained. The pronounced splitting of the characteristic double peak near $2\theta = 70°$ indicates well-ordered, layered materials.

In Fig. 6, the ratio c/a of the hexagonal cell parameters c and a is plotted versus the content of dopants for both, the aluminum- and the magnesium-doped mixed oxides. This crystallographic cell parameter ratio is a direct measure for

the well-ordered, layered character of the structure. For each sample series of increased cobalt content, the c/a ratio is increased. Thus, cobalt increases the c/a ratio and stabilizes the layered crystal structure arrangement. For all sample
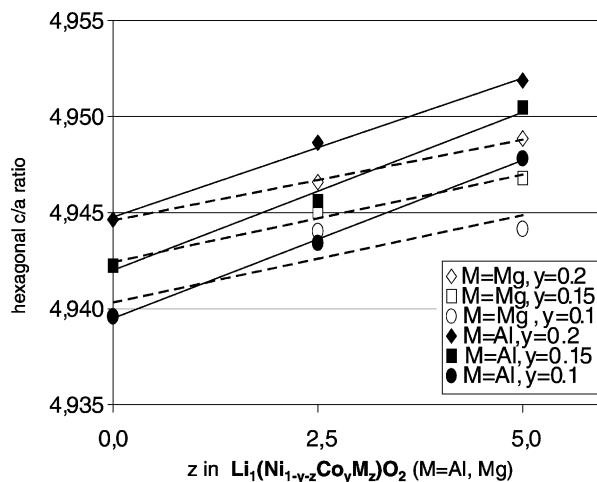

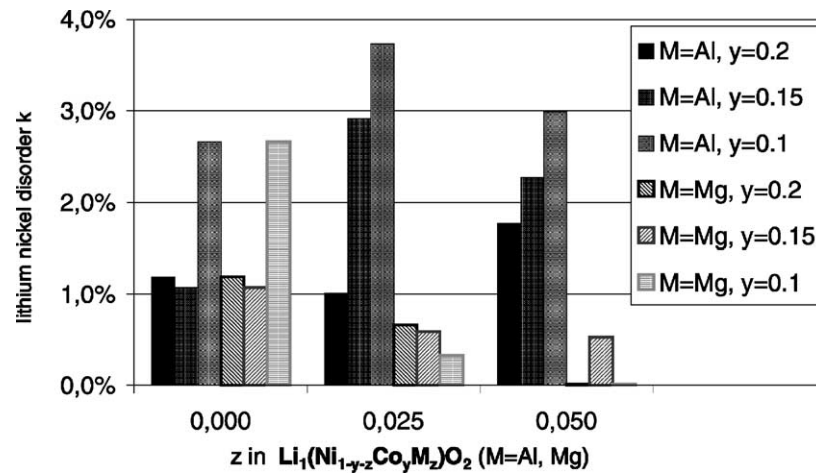Fig. 6. Ratio c/a of the hexagonal cell parameters for aluminum- and magnesium-doped mixed oxides, Li(Ni$_{1-y-z}$Co$_y$M$_z$)O$_2$ (M = Al, Mg), in dependence on the content of dopants.

Fig. 7. Lithium nickel disorder for aluminum- and magnesium-doped mixed oxides, $Li(Ni_{1-y-z}Co_yM_z)O_2$ (M = Al, Mg), in dependence on the content of dopants.

series, the c/a ratio also increases with increasing aluminum or magnesium content. This rise is steeper for aluminum than for magnesium. Therefore, aluminum and magnesium both stabilize the layered crystal structure arrangement of the mixed oxide materials; the impact of aluminum is more pronounced than the impact of magnesium.

The lithium nickel disorder k of the mixed oxides is depicted in Fig. 7 as a function of the aluminum and magnesium content. The data are divided into series of constant cobalt content. Since the Rietveld analysis of the XRD data is not that sensitive with regard to lithium, there is a significant experimental scattering of the data. Nonetheless, there is an overall decrease of the disorder with increased cobalt content for both, aluminum- and magnesium-doped materials. The aluminum content has no clear effect though. In the case of magnesium-doped mixed oxides, however, the lithium nickel disorder seems to decrease strongly with increasing magnesium content.

All refinements converged to the preferred occupation of lithium positions by magnesium instead of nickel, leading to lower lithium nickel disorder. But the improvement of the quality of fit is not very pronounced, arising from the fact, that the difference in X-ray scattering power between nickel and magnesium is not sufficient for a clear distinction between the structural models. There are also results of magnetic measurements on magnesium-doped lithium nickel oxide, which strongly confirm a preferential substitution of lithium by magnesium instead of nickel [10].

3.3. Cycling test

Fig. 8 shows the cycle behavior of a selection of materials versus MCMB-6-28 graphite in a 2025 full coin cells. The expression, first generation, represents binary lithium nickel cobalt oxides, whereas second generation represents materials that are additionally doped with Al. The cycling
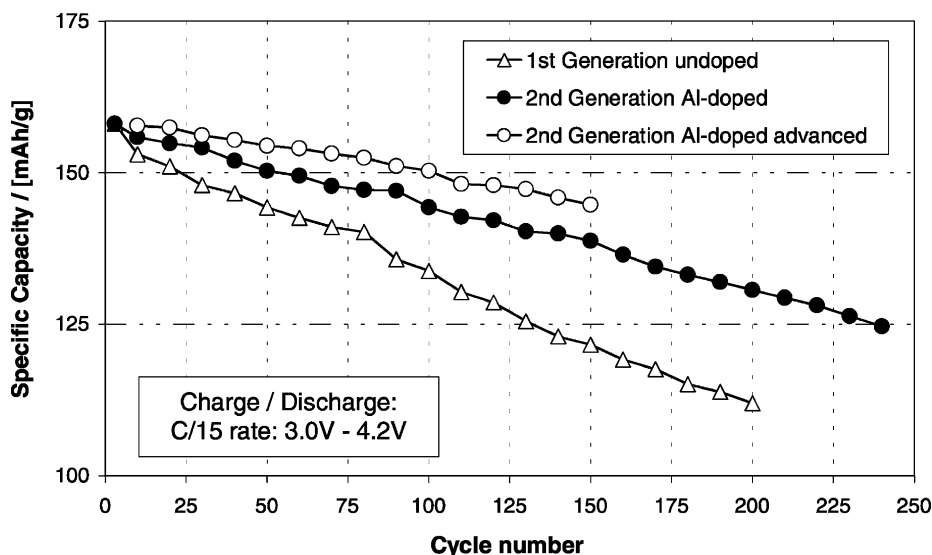

Fig. 8. Cycling test of $Li(Ni_{1-y-z}Co_yM_z)O_2$ vs. graphite in coin cells, type 2025.
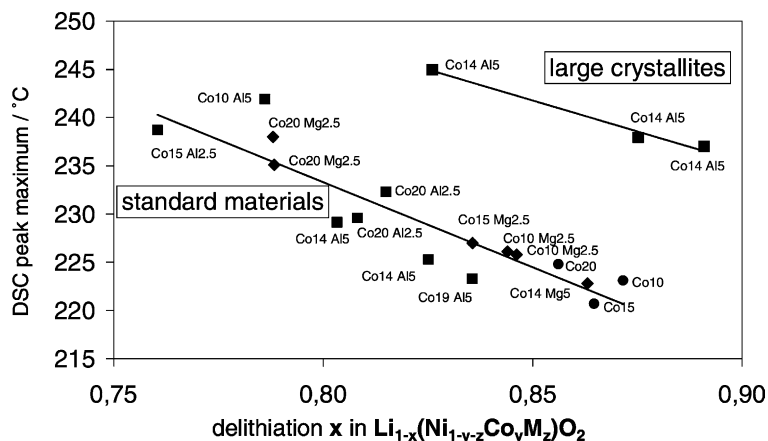
Fig. 9. Decomposition temperature of lithium nickel cobalt mixed oxide electrodes charged to 4.3 V and washed free of electrolyte, in dependence on the state of delithiation x in $Li_{1-x}(Ni_{1-y-z}Co_yM_z)O_2$ (M = Al, Mg). (●) Co; (■) Co–Al; (◆) Co–Mg.

stability of lithium nickel cobalt oxide materials could be significantly improved by Al doping. Within the composition range of the phase diagram displayed in Fig. 1, a correlation between Al content and cycling stability has been determined.

3.4. Thermal measurements

Simultaneous DSC and TG scans were performed on mixed oxide electrodes that were potentiostatically charged to 4.3 V versus Li/Li$^+$, and were cleaned of electrolyte. For the evaluation of the scans, the characteristic exothermic reaction occurring between 200 and 250 °C, accompanied by weight loss, was considered. In Fig. 9, the respective decomposition temperature, i.e. the maximum of the DSC peak, is plotted versus the state of delithiation x in Li_{1-x} $(Ni_{1-y-z}Co_yM_z)O_2$ (M = Al, Mg). The state of delithiation is derived from the total charge/discharge balance of the electrode. For the samples synthesized under the standard conditions of the applied process, there is an approximately linear correlation between decomposition temperature and state of delithiation. This correlation exists independent of the doping element. Aluminum and magnesium doping cause a shift of the corresponding data points towards the low delithiation degree—high decomposition temperature side of this correlation. Thus, it can be concluded that an increased thermal stability by aluminum or magnesium doping is rather an indirect effect due to limited delithiation than a direct effect caused by structural or thermochemical stabilization (at least for the experimental settings of this study). On the other hand, materials comprising large crystallite sizes of the kind shown in Fig. 3b, build up a second linear correlation, which is parallelly moved to higher decomposition temperatures. Obviously, an enlargement of the crystallites increases the decomposition temperature, independent of the delithiation state.

In order to confirm that the correlation of decomposition temperature and delithiation state is independent of alumi-

num doping, a further experiment was performed. In this experiment, an undoped mixed oxide, $Li(Ni_{0.85}Co_{0.15})O_2$, and an aluminum-doped one, $Li(Ni_{0.80}Co_{0.15}Al_{0.05})O_2$, were each charged to a defined delithiation state. In Fig. 10, some
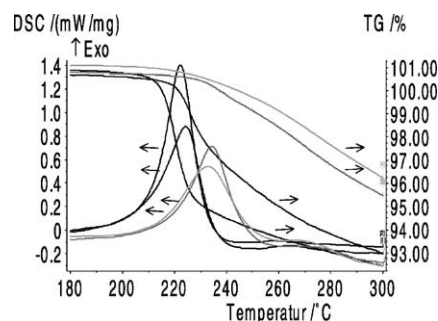

Fig. 10. DSC and TG curves of two mixed oxides $Li_{1-x}(Ni_{1-0.15-z}Co_{0.15}Al_z)O_2$ ($z = 0$ and 0.05), each charged to various delithiation states x: (—) $Li_{1-0.875}(Ni_{0.85}Co_{0.15})O_2$; (-) $Li_{1-0.875}(Ni_{0.80}Co_{0.15-}Al_{0.05})O_2$; (–) $Li_{1-0.75}(Ni_{0.85}Co_{0.15})O_2$; (–) $Li_{1-0.75}(Ni_{0.80}Co_{0.15}Al_{0.05})O_2$.
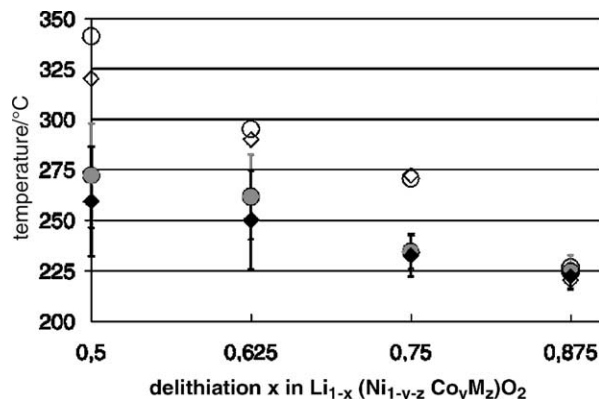

Fig. 11. Thermal parameters of two mixed oxides, $Li_1(Ni_{1-0.15-z}Co_{0.15}Al_z)O_2$ ($z = 0$ and 0.05), in dependence on delithiation state x in $Li_{1-x}(Ni_{1-y-z}Co_yAl_z)O_2$. TG inflexion point (○) $z = 0$, (◇) $z = 0.05$; DSC peak maximum (◉) $z = 0$, (◆) $z = 0.05$; DSC peak width (I) $z = 0$ and 0.05.

of the corresponding TG and DSC scans are shown. The thermal scans for the two materials do not differ significantly, when they are compared for identical delithiation states, whereas there are distinct differences, when different delithiation states are compared for one material. In Fig. 11, this fact is more clearly depicted in a quantified way. In this figure, some thermal parameters, derived from the thermal scans, are plotted versus the delithiation state x. The TG point of inflection, the DSC peak maximum and the DSC peak width decrease linearly with increased delithiation. Indeed, the respective correlations do not differ significantly for the tested materials, $Li(Ni_{0.85}Co_{0.15})O_2$ and $Li(Ni_{0.80}Co_{0.15}Al_{0.05})O_2$.

4. Conclusions

Phase pure, spherical, aluminum- and magnesium-doped lithium nickel cobalt mixed oxides, $Li_{1-x}(Ni_{1-y-z}Co_yM_z)O_2$ (M = Al, Mg), of a well-ordered layered structure have been successfully synthesized by applying the industrial synthesis process developed by H.C. Starck. The spherical powder particles are composed of regular crystallites. The size of the latter can be controlled by the synthesis temperature. Cobalt, aluminum and magnesium all stabilize the layered structure. The lithium nickel disorder is decreased by cobalt doping and nearly unaffected by aluminum doping. According to the Rietveld refinements, magnesium seems to reduce the lithium nickel disorder strongly, though refinements need to be considered carefully. Both, aluminum and magnesium doping enhance the cycling stability of lithium nickel cobalt mixed oxides. The decomposition temperature of charged electrodes without electrolyte is rather a function of the delithiation state than of aluminum or magnesium content.

Therefore, aluminum and magnesium enhance the thermal stability of the delithiated phase mainly by an intrinsic limitation of the delithiation. However, a stabilizing effect independent of delithiation can be achieved by an enlargement of the crystallite size.

References

[1] T. Ohzuku, H. Komori, K. Sewai, T. Hirai, Chem. Express. 5 (1990) 733.
[2] C. Delmas, I. Saadoune, Solid State Ionics 53–56 (1992) 370.
[3] M. Okada, K.-I. Takahashi, Takashi Mouri, J. Power Sources 68 (1997) 545.
[4] J. Cho, H. Jung, Y.C. Park, G.B. Kim, H.S. Lim, J. Electrochem. Soc. 147 (2000) 15.
[5] T. Ohzuku, A. Ueda, M. Kouguchi, J. Electrochem. Soc. 142 (1995) 4033.
[6] T. Ohzuku, T. Yanagawa, M. Kouguchi, A. Ueda, J. Power Sources 68 (1997) 131.
[7] Q. Zhong, U. von Sacken, J. Power Sources 54 (1995) 221.
[8] Y.-I. Jang, B. Huang, H. Wang, G.R. Maskaly, G. Ceder, D.R. Sadoway, Y.-M. Chiang, H. Liu, H. Tamura, J. Power Sources 81/82 (1999) 589.
[9] C.-C. Chang, J.Y. Kim, P.N. Kumta, J. Electrochem Soc. 147 (2000) 1722.
[10] C. Pouillerie, L. Croguennec, Ph. Biensan, P. Willmann, C. Delmas, J. Electrochem. Soc. 147 (2000) 2061.
[11] J. Cho, B. Park, J. Power Sources 92 (2001) 35.
[12] U. Krynitz, W. Kummer, M. Benz, J. Meese-Marktscheffel, E. Pross, V. Stoller, WO 98/37023.